Available online at www.sciencedirect.com
SCIENCE DIRECT®
International Journal of Thermal Sciences 43 (2004) 743–752
International Journal of Thermal Sciences
www.elsevier.com/locate/ijts

Movement of maximum heat flux and wetting front during quenching of hot cylindrical block

Jaffar Hammad, Yuhichi Mitsutake, Masanori Monde *

Department of Mechanical Engineering, Saga University, 1 Honjo-machi, Saga-shi, Saga 840-8502, Japan

Received 20 August 2003; received in revised form 18 December 2003; accepted 24 February 2004

Available online 25 May 2004

Abstract

An experimental work is carried to study the characteristics of heat transfer and wetting front during quenching high temperature cylindrical block by water jet at atmospheric pressure. The surface temperature and heat flux are estimated by applying a two-dimensional inverse solution. The movements of both wetting front and transition boiling region over the heated block surface were observed using a high speed video camera. The surface temperature and heat flux over the whole surface during quenching could be estimated well. The surface temperature, the position and the time at which the maximum heat flux occurs are obtained. It has been found that the maximum heat flux occurs neither in the wetting front, nor in the transition boiling region but in the fully wetted region. It has also been found that the maximum heat flux dose not start at the same time when the jet water strikes the heated block, but it starts when the surface temperature decreases to a value less than 170 °C.

Keywords: Inverse solution; Impinging jet; Quenching; Two-dimensional transient heat conduction

1. Introduction

It is important to understand the characteristics of heat transfer and the wetting front during quenching of a high temperature solid with an impinging liquid jet. In many applications that use water to cool high temperature surfaces, surface heat flux and temperature rapidly change with the wetting front during quenching. Such applications include industrial processes which involve strip steel on a run-out table [1], continuous casting [2,3], and forging [4]. For example, the product quality from manufacturing processes depends on thermal response of material to the cooling methods that are employed during manufacturing. The product quality does only include physical dimensions, but also mechanical properties. Another application is the safe operation of water-cooled nuclear reactors; it is necessary to predict accurately the rate of heat removal from fuel elements during a loss of coolant accident (LOCA) [5,6]. To prevent the cladding from overheating and to reestablish convection wet-wall cooling, water is injected in the hot reactor core. However, due to heat decay in the fuel element, the cladding surface temperature increases above the rewetting temperature which leads to a stable vapor blanket that prevents the immediate return to liquid–solid contact. Rewetting is the re-establishment return of liquid contact with a hot cladding surface and, thereby, bringing it to an acceptable temperature. Several experimental and analytical investigations [7,8] have been conducted to understand film boiling heat transfer of water jets impinging on high temperature flat plates with a focus on the jet stagnation zone and to control the surface temperature. Filipovic et al. [9] studied the regimes of boiling for quenching phenomena by using nickel-plate copper, which was preheated to an initial temperature exceeding 700 °C and, subsequently, quenched with a parallel water wall jet. They found that the front was at the leading edge of a transition boiling zone and was approximately coincident with location of the maximum heat flux. The location of the maximum heat flux at the hot surface during quenching is very important for understanding the behavior of quenching phenomena. Most of the researchers [9–13] have found that the maximum heat flux occurred at the location of the wetting front position. Other researcher [14,15] found that the maximum heat flux occurs where nucleate boiling occurs.

* Corresponding author. Fax: +952-28-8587.
E-mail address: monde@me.saga-u.ac.jp (M. Monde).

1290-0729/$ – see front matter
doi:10.1016/j.ijthermalsci.2004.02.014

Nomenclature

a	thermal diffusivity	$m^2 \cdot s^{-1}$	
$f(\tau, \gamma, \zeta_n)$	function for approximating temperatures on plane $\zeta = \zeta_n$ inside solid		
$G_{j,k}^{(m,n)}$	coefficient in Eq. (2)		
$H_{j,k}^{(m,n)}$	coefficient in Eq. (3)		
h	heat transfer coefficient, $= q_w/(T_w - T_{liq})$	$kW \cdot m^2 \cdot °C^{-1}$	
h_{max}	maximum heat transfer coefficient	$kW \cdot m^{-2} \cdot °C^{-1}$	
h_s	heat transfer coefficient predicted in steady state condition	$kW \cdot m^{-2} \cdot °C^{-1}$	
$J_0(r)$, $J_1(r)$	Bessel function		
k	thermal conductivity		
l_r	length in r direction of a cylindrical coordinate		
l_z	length in z direction of a cylindrical coordinate		
m_j	eigenvalue (root of $J_1(m_j) = 0$)		
N	degree of approximate polynomial		
N_j	degree of eigenvalue		
$P_{j,k}^{(n)}$	coefficient derived from measured temperature		
q_{max}	maximum heat flux	$MW \cdot m^{-2}$	
q_w	surface heat flux	$MW \cdot m^{-2}$	
r	radius	mm	
r_h	position for maximum heat transfer coefficient	mm	
r_w	position for wetting front	mm	
r_q	position for maximum heat flux	mm	
r_s	position for stop boiling region	mm	
t	time	sec	
T	measured temperature		
T_{int}	initial temperature of block	°C	
T_{liq}	liquid temperature	°C	
T_{sat}	saturated temperature	°C	
ΔT_{sub}	liquid subcooling $(T_{sat} - T_{liq})$	°C	
T_w	surface temperature	°C	
T_w^*	surface temperature at maximum heat flux	°C	
u_j	jet velocity	$m \cdot s^{-1}$	
z_1, z_2	the distance of thermocouples location from the hot surface	mm	
z	z-coordinate distance	mm	

Greek symbols

γ	non-dimensional distance in r-direction, $= r/l_r$
δ_v	vapor layer thickness
ζ	non-dimensional distance in z-direction, $= z/l_z$
θ_w	non-dimensional surface temperature, $= T/T_{int}$
τ	non-dimensional time, $= at/l_r^2$
τ_n^*	non-dimensional time lag
Φ_w	non-dimensional surface heat flux

Theoretical and experimental studies are still needed since the wetting process involves a large number of sub-processes that are themselves complicated and very difficult to investigate. In addition, during the quench the surface temperature and heat flux sharply changes with the wetting front. In the most of researches, the surface temperatures were not estimated with high accuracy from the measured temperatures in the solid. The solution method for two-dimensional inverse heat conduction problems, IHCP, which was recently developed by Monde et al. [16], makes it possible to successfully estimate surface temperature and heat flux from the measured temperatures in the solid. Monde et al. [16] determined the surface temperature and heat flux analytically for a homogeneous rectangular body, and could predict them well over the whole surface with an error less than a few percent. Hammad et al. [17] applied the same analytical solution of Monde et al. [16] to determine the surface temperature and heat flux for a cylindrical body and obtained good results. In this current research we used the same method to determine the surface temperature and heat flux during the quenching of a cylindrical block. The temperatures at different points inside the high temperature body were measured and, at the same time, a high speed video camera observed the propagation of the wetting front and boiling region flow over the hot surface. The estimated surface heat condition, which is based on the measured temperatures inside the heated body, in conjunction with the observation made to the movement of liquid on the surface allowed us to better understand the quenching phenomena.

The main objectives of the present research are to:

(1) determine the surface temperature and heat flux by applying two-dimensional inverse solution during quenching,
(2) measure the size and position of the boiling region and the wetting front which moves with time,
(3) find the position at which the maximum heat flux occurs, and
(4) determine the value of the surface temperature at which the maximum heat flux occurs.

2. Experimental setup

The experimental apparatus, as shown in Fig. 1, consists of four major parts:

(a) heated block capsule;
(b) liquid circulation system;
(c) data acquisition system; and
(d) high-speed video camera.

Referring to Fig. 1, the experimental procedure is accomplished as follows:

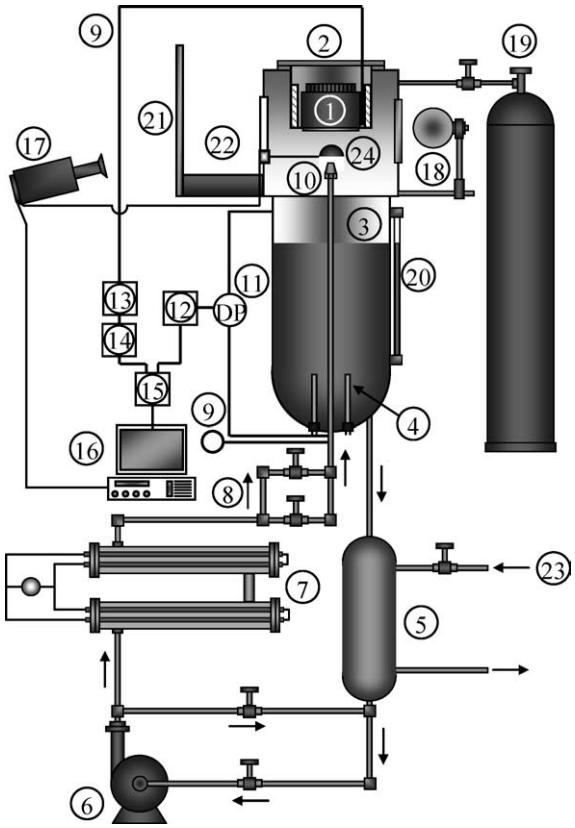

Fig. 1. Schematic of the experimental setup: (1) Tested block; (2) Block holder; (3) Liquid tank; (4) Heater; (5) Cooling jacket; (6) Pump; (7) Auxiliary heater; (8) Regulating valve; (9) Thermocouple; (10) Nozzle; (11) Differentail pressure; (12) Dynamic starin meter; (13) Ice box; (14) Voltage amplifier; (15) A/D converter; (16) Computer; (17) High-speed video camera; (18) Spot light; (19) Nitrogen cylinder; (20) Level gauge; (21) Glass frame; (22) Vessel; (23) Cooling water; (24) Rotary shutter.

The water container (3) is filled with distilled water up to a certain level which is observed by the level gauge (20). Water fills all the pipelines up to the pump inlet. The regenerative pump (6), then, pumps the water so that it exits out of the nozzle (10). The position of the nozzle is fixed by an adjustable device in such a way that the water jet (10) can strike exactly at the center of the block (1). A shutter (24) is mounted in front of the nozzle to prevent water from striking the block (1) prematurely and to maintain a constant water temperature by forcing it to run within a closed loop system. The desired temperature of the water is obtained by controlling the main heater (4) and auxiliary heater (7). The initial temperature of the block (1) is achieved by an electrical heater that is mounted around the block. The velocity of the water jet is regulated by a regulating valve (8). Nitrogen gas is fed around the heated surface block by opening the cylinder valve (19) to remove oxygen away from the heated surface and, consequently, prevent oxidization from taking place. When all the desired experimental conditions are fulfilled then the shutter (24) is removed and the water jet strikes the center of the heated block. The high speed video camera (17) records the wetting front over the heated block surface at the same time the 16 thermocouples measure the temperatures inside the heated block. Table 1 shows the different conditions investigated in the experiments.

Table 1
Experimental conditions

Material of block	Initial temperature T_{int} [°C]	Liquid subcooling ΔT_{sub} [°C]	Jet velocity u_j [m·s^{-1}]
Copper	250		
Brass	300	5	3
Steel		20	5
		50	10
		80	15

The values in Table 1 are only representatives, i.e., the initial temperature of 300 °C corresponds to the range 299 to 305 °C, while the initial temperature of 250 °C corresponds to the range 249 to 255 °C. The subcooling of 5, 20, 50 and 80 °C involve an uncertainty of $+2$ °C and -1 °C. The jet velocities of 3, 5, 10 and 15 m·s^{-1} involve an uncertainty of ± 0.2 m·s^{-1}.

In this paper we will focus on one condition only that is summarized as: the material is brass, the initial temperature is $T_{\text{int}} = 300$ °C, the jet velocity is $u_j = 5$ m·s^{-1}, and the subcooling is $\Delta T_{\text{sub}} = 50$ °C. For the sake of comparison we will present the data of other conditions when necessary.

Heated block. The heated block is of cylindrical shape with 94 mm diameter and 59 mm height. In order to make it easy to fix the thermocouples inside the heated block, a part of it was removed; but it has no effect on the heat transfer within a region of $r \leqslant 30$ mm. The 16 thermocouples (CA-type, 1 mm diameter) are located at two different distances from the heated surface block; 2.1 mm and 5 mm. At each distance, eight thermocouples are inserted in the drill-made channels, with 1 mm diameter, inside the block in the r-direction until being embedded in the center of the cylinder block. To protect the boiling surface from oxidation, the block surface was coated with a thin layer of gold, 16 μm, which has an excellent oxidation resistance characteristic and also a good thermal conductivity; $k \approx 317$ W·m^{-1}·K^{-1}. The surface roughness is 0.2–0.4 μm. Hence, the effect of surface roughness on film boiling can be neglected. Fig. 2 shows the assembly of the block, where it is mounted in a block holder and is heated by an electrical sheath heater with 0.94 kW capacity, that is wrapped around the block circumference. For thermally insulating the block and to keep a uniform heat flux at the surfaces, two auxiliary heaters are used; one of them is of band type, 0.65 kW, and is placed around the block circumference, while the second is of slot type, 0.5 kW, and is placed in the four groves in the upper part of the block as illustrated in Fig. 2.

Data acquisition system. A data acquisition system was used to record the measured temperatures in the block. The thermocouples are scanned sequentially at 0.05 sec intervals,

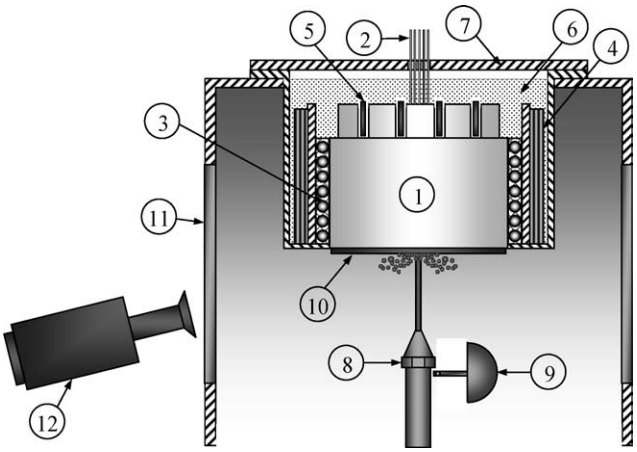

Fig. 2. Schematic of assembling block heater placement: (1) Tested block; (2) Thermocouples; (3) Sheath heater; (4) Band type heater; (5) Slot type heater; (6) Glass wool; (7) Block holder; (8) Nozzle; (9) Rotary shutter; (10) Hot surface; (11) Glass window; (12) High speed video camera.

with 8.0 ms needed to read all of the thermocouples using 16-bit resolution with an analog-digital converter. The duration of the total data acquisition period depends on parameters such as the impingement velocity, u_j, subcooled temperature, ΔT_{sub}, block initial temperature, T_{int}, and type of block material. The uncertainty in the temperature measurements is $\pm 0.1\,^{\circ}\text{C}$, while the uncertainty in the placement of the thermocouples is estimated to be ± 0.1 mm. The time lag for the response of the thermocouples is estimated to be less than 0.1 sec.

Visual observation. The quenching of the heated surface was recorded using a high-speed video camera. This camera is capable of recording pictures with a resolution of 572×434 pixels and has a maximum frame rate of 12400 frames·second^{-1}. The video images were divided into pictures for short intervals of time to allow us to measure the observed wetting front and transition boiling positions. The error in this measurement is ± 0.18 mm.

3. Analysis of experimental data

Because the direct measurement of the surface temperature usually becomes impossible during quenching, the Inverse Heat Conduction Problem (IHCP) technique is used to determine surface temperature and heat flux from measured temperature inside a body. In this paper we used two-dimensional inverse solution method [16,17] of a cylindrical coordinator which was already developed to determine surface conditions in non-dimensional form. The mathematical analysis of this case is based on that the circumference of the cylinder is thermally insulated, so that no heat transfer takes place with the surrounding, while the upper and lower surface are not insulated. Therefore, two measured points at two different depths from the surface are needed to estimate surface condition by applying two-dimensional inverse solution. The procedure for calculating the surface temperature and heat flux by implementing two-dimensional inverse solution method [17] is explained briefly as follows: first, the experimental parameters should be converted to non-dimensional ones in order to perform the analysis. Fig. 3 shows the variation of the measured temperature by the 8 thermocouples at the depth $z_1 = 2.1$ mm from the surface. For the convenience of the calculation procedure additional points were interpolated between the measured points by implementing the smooth Splines method, so that the number of reference points was increased from 8 to 29. The same procedure was followed for the measured temperature at the depth $z_2 = 5$ mm. Then we inserted the measured temperatures after interpolation for each distance in the following approximate equation:

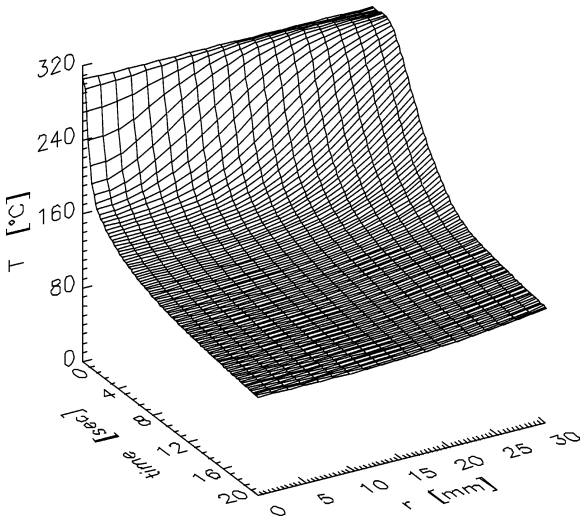

Fig. 3. Measured temperature data at $z_1 = 2.1$ mm (Brass, $T_{\text{int}} = 300\,^{\circ}\text{C}$, $\Delta T_{\text{sub}} = 50\,^{\circ}\text{C}$, $u_j = 5$ m·s^{-1}).

$$f(\tau,\gamma,\zeta_n) = \sum_{j=0}^{N_j} J_0(m_j\gamma)\cdot\sum_{k=0}^{N}\frac{P_{j,k}^{(n)}\cdot(\tau-\tau_n^*)^{k/2}}{\Gamma(k/2+1)} \quad \text{at } n=1,2 \tag{1}$$

The coefficients $P_{j,k}^{(n)}$ were then determined from the measured temperatures using the least mean square method. The obtained values of $P_{j,k}^{(n)}$ were then inserted into Eq. (1) to get the corresponding reproduced temperature curves for the two depths to check the applicability of these coefficients. By comparing the measured temperature with the reproduced temperature a good agreement is obtained which indicates that $P_{j,k}^{(n)}$ are reliable and therefore, can be used in the calculation of the surface condition. The following Eqs. (2) and (3) are used to calculate the surface temperature and heat flux, respectively:

$$\theta_w(\tau,\gamma) = \sum_{j=0}^{N_j}\sum_{\ell=-1}^{N} G_{j,\ell}^{(1,2)}\cdot\frac{(\tau-\tau_1^*)^{\ell/2}}{\Gamma(\ell/2+1)}\cdot J_0(m_j\gamma) - \sum_{j=0}^{N_j}\sum_{\ell=-1}^{N} G_{j,\ell}^{(2,1)}\cdot\frac{(\tau-\tau_2^*)^{\ell/2}}{\Gamma(\ell/2+1)}\cdot J_0(m_j\gamma) \tag{2}$$

$$\Phi_w(\tau,\gamma) = \sum_{j=0}^{N_j}\sum_{\ell=-1}^{N} H_{j,\ell}^{(1,2)} \cdot \frac{(\tau-\tau_1^*)^{\ell/2}}{\Gamma(\ell/2+1)} \cdot J_0(m_j\gamma) - \sum_{j=0}^{N_j}\sum_{\ell=-1}^{N} H_{j,\ell}^{(2,1)} \cdot \frac{(\tau-\tau_2^*)^{\ell/2}}{\Gamma(\ell/2+1)} \cdot J_0(m_j\gamma) \quad (3)$$

where $J_0(m_j\gamma)$ is the Bessel function, m_j is the eigenvalue and $G_{j,k}^{(m,n)}$ and $H_{j,k}^{(m,n)}$ are constants. The symbol τ_n^* is the time lag which is the time needed for a temperature to be monitored at the measuring point. It can be determined by setting $\operatorname{erfc}(\gamma_n/2\sqrt{\tau_n^*}) = \min(\theta)$, where $\min(\theta)$ is a minimum readable division of measured temperature. There are two reasons that allow us to adopt the form of half polynomial series of time: (1) the general solution of heat conduction possesses the item of root of time and (2) the one-dimensional IHCP, which uses the form of half polynomial series of time in temperature approximation, has achieved success. More details about Eqs. (1), (2), and (3) can be found in the work of Hammad et al. [17].

4. Results and discussion

The number of the measured temperatures in the solid is numerically verified to be eight enough for Eqs. (2) and (3) to estimate the surface temperature and heat flux with satisfactory accuracy [16,17]. Figs. 4 and 5 show the surface temperature estimated using Eq. (2) and the surface heat flux estimated using Eq. (3), respectively. As we see, the surface temperature and heat flux seem physically reasonable, where heat flux and temperature decrease smoothly over the hot surface during quenching. In Fig. 4, the track of the maximum surface heat flux, $q_{\max}$, is shown by a solid line on the heat flux surface plane on which it decreases gradually with time and position. In Fig. 5, the surface temperature at $q_{\max}$ is shown by a solid line on the temperature surface plane, on which its value falls in the range of 140–168 °C. On the $r-t$ plane in Figs. 4 and 5, the positions of maximum heat flux, r_q, and the observed wetting front, r_w, are shown by a solid line and dashed line, respectively. The positions r_q and r_w are very close during the cooling of the hot surface. In addition, the position r_q appears after the surface is wetted, since it is following the position, r_w.

Flow situation. During the quench, the flow situation at the time, $t = 2.7$ sec for example, is observed as shown in Fig. 6 where the wetting front spreads towards the circumference with time. From the image in Fig. 6 we can recognize three different regimes in the flow situation: the first is no splashed droplets, the second is splashed droplets generated by strong vapor ejection, and the third is disappearance of the droplets, that is the apparently dry area. The boundaries of the three regimes can be identified at the locations of r_s and r_w based on the observation. The position of r_w can be called the wetting front. In the region between r_s and

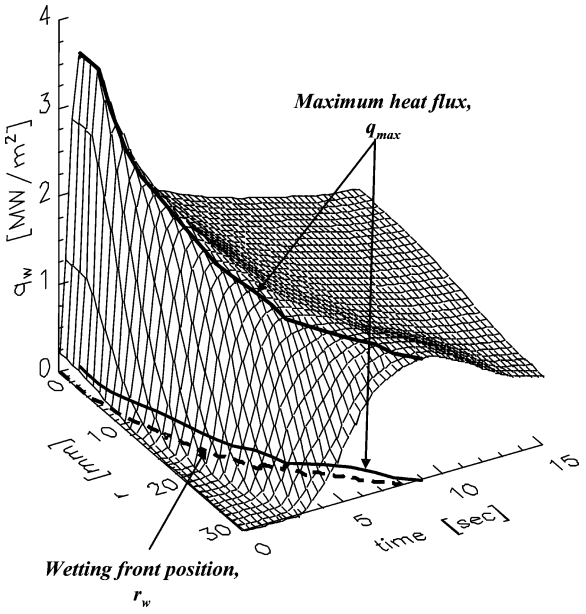

Fig. 4. Surface heat flux graph (Brass, $T_{\text{int}} = 300\,^\circ\text{C}$, $\Delta T_{\text{sub}} = 50\,^\circ\text{C}$, $u_j = 5\ \text{m}\cdot\text{s}^{-1}$).

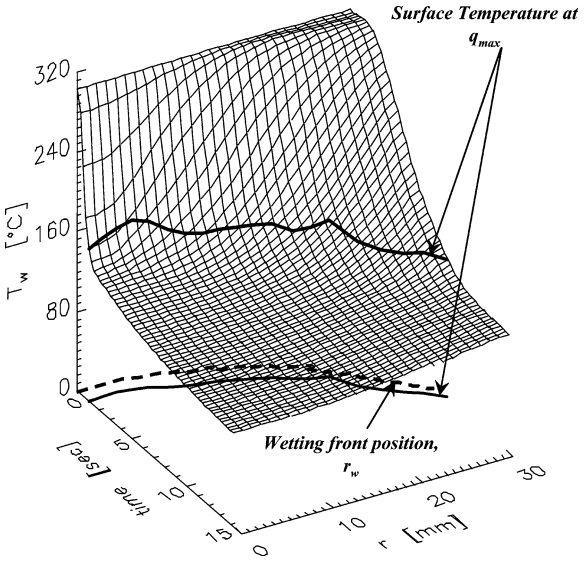

Fig. 5. Surface temperature graph (Brass, $T_{\text{int}} = 300\,^\circ\text{C}$, $\Delta T_{\text{sub}} = 50\,^\circ\text{C}$, $u_j = 5\ \text{m}\cdot\text{s}^{-1}$).

r_w, the heat transfer changes from film boiling to nucleate boiling that is its region corresponds to transition boiling. At the same selected time, the surface temperature, T_w, heat flux, q_w, and heat transfer coefficient, h, are also calculated from Eqs. (2) and (3). For a comparison of transient heat transfer coefficient, the steady state heat transfer coefficient for single-phase flow, h_s, is calculated from the correlation proposed by Liu et al. [18]. By combining the observed image and the surface conditions as shown in Fig. 6, we can determine the values of T_w, q_w and h at the positions r_w and r_s, and then the position, r_q, at which the maximum heat flux, $q_{\max}$ occurs, can be determined. The position

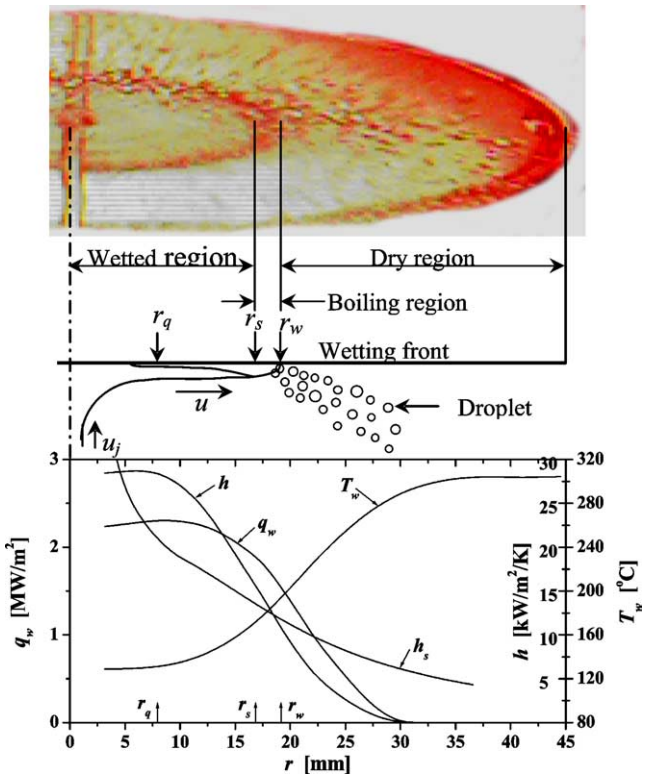

Fig. 6. The positions r_q, r_s and r_w at specific time ($t = 2.7$ sec) on the flow boiling aspect and the values of q_w, T_w, h and h_s for each position (Brass, $T_{\text{int}} = 300\,^{\circ}\text{C}$, $\Delta T_{\text{sub}} = 50\,^{\circ}\text{C}$, $u_j = 5\ \text{m}\cdot\text{s}^{-1}$).

r_q is not located within the transient boiling region and appears in the range of $r < r_s$. The temperature T_w at r_q is significantly greater than the saturated temperature at atmospheric pressure which indicates that a thin layer of bubbles is formed on the surface between r_q and r_s. The bubbles in this thin layer quickly condense when they emerge within the single phase flow, which may make the layer difficult to be observed. The intersection point between h and h_s curves can show the position of the single phase flow region on the surface.

The positions; r_w, r_s, r_q and the position r_h which corresponds to the maximum heat transfer coefficient $h_{\max}$ are plotted against time as shown in Fig. 7. The transition boiling region between r_w and r_s are increased over the hot surface during quenching. This means that the bulk liquid temperature increases in the flow direction. At the beginning, the water jet strikes the hot surface and then r_w and r_s suddenly expand, while r_q and r_h occur after certain periods of time. For example, at the position $r = 5$ mm, r_w and r_s first take place and then r_q occurs after 1.4 sec while r_h occurs after 2.3 sec as shown in Fig. 7.

Surface heat flux and temperature. Fig. 8 shows the surface heat flux and surface temperature at different selected positions with time, where surface heat flux increases until reaching a maximum value then decreases with time for each position. The surface temperature decreases sharply at the beginning, and then continues decreasing gradually as shown in Fig. 8.

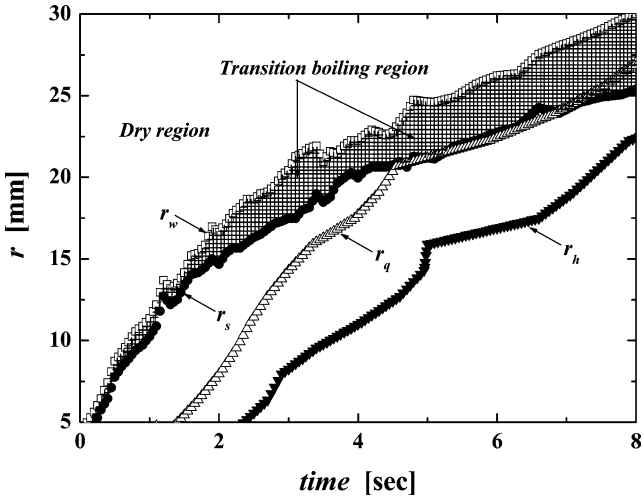

Fig. 7. Positions of r_q, r_h, r_s and r_w according to the time (Brass, $T_{\text{int}} = 300\,^{\circ}\text{C}$, $\Delta T_{\text{sub}} = 50\,^{\circ}\text{C}$, $u_j = 5\ \text{m}\cdot\text{s}^{-1}$).

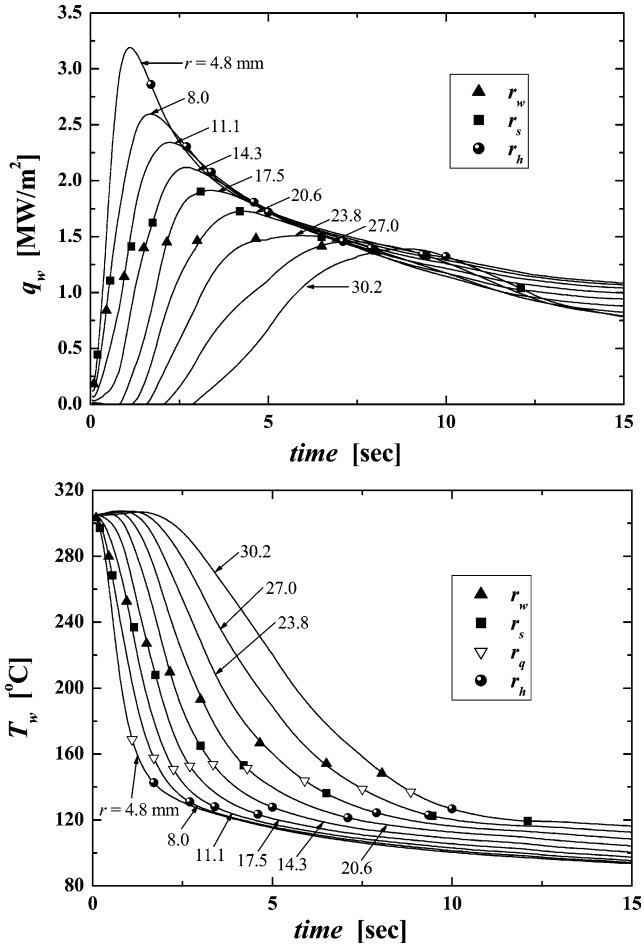

Fig. 8. Surface heat flux and surface temperature as a function of time (Brass, $T_{\text{int}} = 300\,^{\circ}\text{C}$, $\Delta T_{\text{sub}} = 50\,^{\circ}\text{C}$, $u_j = 5\ \text{m}\cdot\text{s}^{-1}$).

The values of surface heat flux and temperature at r_w, r_s and r_h are shown in Fig. 8. The transient boiling region

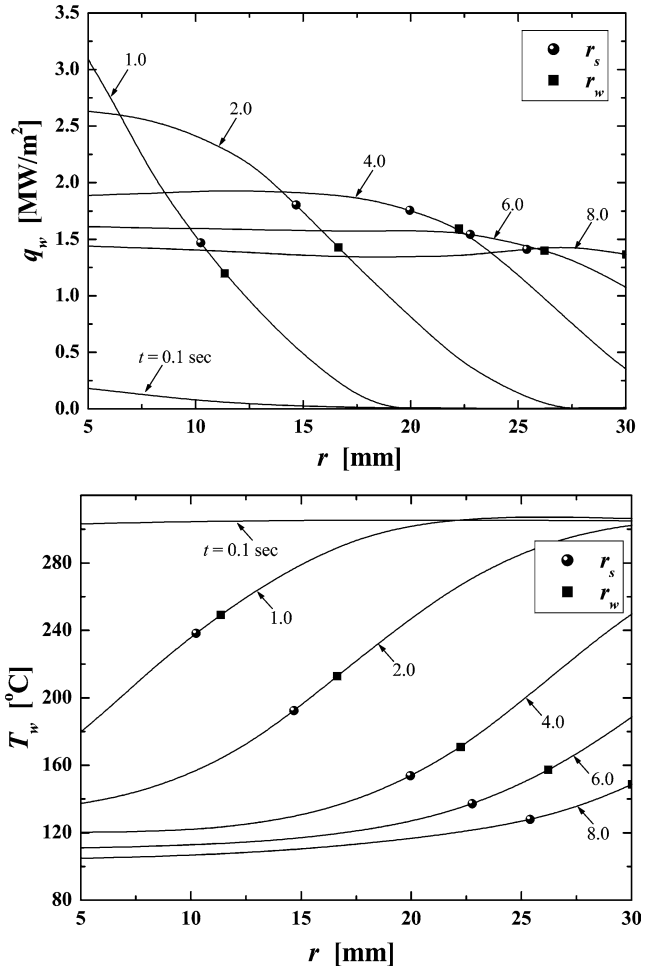

Fig. 9. Surface heat flux and surface temperature as a function of position (Brass, $T_{\text{int}} = 300\,^{\circ}\text{C}$, $\Delta T_{\text{sub}} = 50\,^{\circ}\text{C}$, $u_j = 5\ \text{m}\cdot\text{s}^{-1}$).

occurred between the two positions r_w and r_s, where it increases with increasing surface heat flux and decreasing surface temperature during wetting front movement from position to position with time as shown in Fig. 8. The transient boiling region starts with film boiling which is characterized by a high temperature difference between the surface and the subcooled water, and is accompanied with generating a large number of small size droplets. These droplets become larger in size and their number decreases during film boiling progress over the heated surface. In Fig. 8 we can see that $q_{\max}$ occurs when the surface temperature becomes less than 168 °C, while $h_{\max}$ occurs when the surface temperature is between 120–140 °C. From this figure we can conclude that $q_{\max}$ does not occur at the same time that the jet water strikes the heated block, but it occurs when T_w decreases to a value in the range of 140–168 °C. Fig. 9 shows the surface heat flux and surface temperature as functions of position for different selected times. At 0.1 sec there is not much change in surface temperature and heat flux, while at 1.0 sec the surface temperature decreases and the surface heat flux increases for the same position. In Fig. 9, the transition boiling region between r_s and r_w for different selected times moves with position, and this movement is accompanied with decreasing T_w and increasing q_w. The transition boiling region occurs far from the position of maximum heat flux occurrence when $t = 1.0$ sec, while when $t = 8.0$ sec the maximum heat flux and transition boiling region occur at the same position. The maximum heat flux depends largely on the surface temperature, while the leading edge of transition boiling depends on the surface temperature in addition to other parameters such as jet velocity and liquid temperature.

Heat transfer coefficient. The heat transfer coefficients are calculated from the surface heat flux, q_w, and surface temperature, T_w, as $h = q_w/(T_w - T_{\text{liq}})$. It is found that h increases sharply at the beginning so that it reaches a maximum value, $h_{\max}$, and then decreases very slightly to reach a constant value. The maximum heat transfer coefficient, $h_{\max}$, occurs at a time after the occurrence of $q_{\max}$. In a single phase heat transfer region, heat transfer coefficient h takes constant values.

Wetting mechanism. It is of special interest to understand the heat transfer mechanism and flow situation of the water jet in relation to the hot surface during wetting front movement. Based on, firstly, the liquid flow situation over the hot surface observed by the high speed video camera, and secondly, the heat transfer rates at the surface which are estimated from the inverse solution, we could build an image about the structure of the area between the hot surface and the water jet. According to the observation of the flow situation, the wetting front hardly goes forward until about 4.2 sec after the jet impingement and is limited in the impinging zone. At $t = 4.2$ sec, the surface temperature, surface heat flux and heat transfer coefficient are obtained as shown in Fig. 10(a). This heat flux is less than $q_w = 0.326\ \text{MW}\cdot\text{m}^{-2}$ which is too small at large superheat of $(T_w - T_{\text{sat}}) = 175\,^{\circ}\text{C}$ to make nucleate boiling possible. Therefore, the heat transfer takes place in film boiling in which a vapor layer prevents the liquid from contacting the heated surface. Under this condition, the vapor layer thickness, δ_v, can be assumed from heat conduction in the vapor layer to be approximately $\approx 10\ \mu\text{m}$. We can adopt an image of the flow condition as shown in Fig. 10(a). After $t = 4.2$ sec, the flow aspect dramatically changes so that the wetting front starts going forward. We obtained the surface heat flux, surface temperature and heat transfer coefficient at $t = 5$ sec when the wetting front slightly moves forward. At this time, the heat flux is quickly increased to reach about $2.1\ \text{MW}\cdot\text{m}^{-2}$ at $T_w = 210\,^{\circ}\text{C}$ which is large enough to produce the vapor by nucleate boiling. Fig. 10(b) shows that the heat flux in a range from r_s to r_w is smaller than the maximum heat flux. As a result, this region seems to be not perfectly wetted by liquid. It means that film and nucleate boiling coexist, thus, it is called transition boiling region. In the central region of $r < r_s$, the surface is fully wetted which indicates that it is responsible for the maximum heat flux

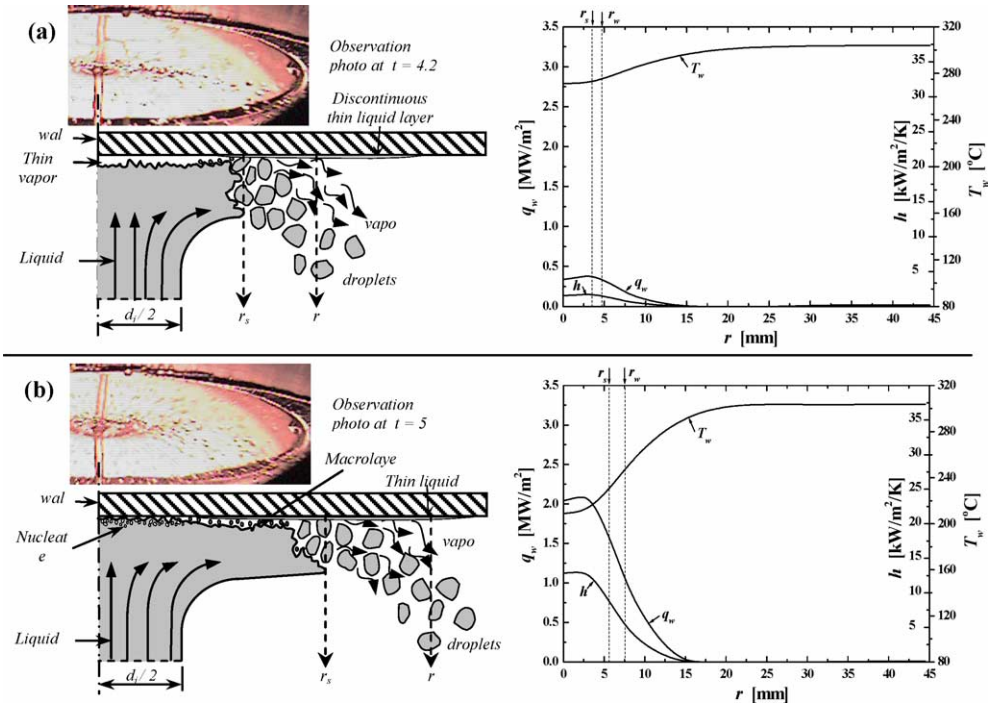

Fig. 10. A model based on flow aspect and measured surface conditions (Brass, $T_{\text{int}} = 300\,^{\circ}\text{C}$, $\Delta T_{\text{sub}} = 50\,^{\circ}\text{C}$, $u_j = 3\ \text{m}\cdot\text{s}^{-1}$, (a) $t = 4.2$ sec, (b) $t = 5$ sec).

occurrence. We finally propose an image of a flow situation as shown in Fig. 10(b), where it continuously shifts in r-direction with time.

Maximum surface heat flux. The maximum surface heat flux moved from one position to another while its value decreased during propagation of the wetted area over the hot surface from the stagnation zone towards the circumference. This maximum heat flux, $q_{\max}$ occurs when T_w decreases to a value less than 170 °C in all the conditions as we saw in Fig. 8. Fig. 11 shows the behavior of $q_{\max}$ as a function of the position, r, for the three materials and the two initial temperatures of 250 and 300 °C at a subcooling of $\Delta T_{\text{sub}} = 80\,^{\circ}\text{C}$ and a jet velocity of $u_j = 10\ \text{m}\cdot\text{s}^{-1}$. We can see in this figure that the type of material affects $q_{\max}$ values in a way that the heat removed from copper is greater than those removed from brass and steel. This can be justified with the help of the thermal conductivity which takes the highest value for copper followed by brass, where steel has the lowest value. The difference in thermal conductivity is reflected in different rates in heat transfer. Fig. 11 also shows that the initial temperature does not have much effect on $q_{\max}$ values.

Fig. 12 shows the time at which $q_{\max}$ occurs as a function of u_j for the copper block at $T_{\text{int}} = 300\,^{\circ}\text{C}$, and $r = 8$ mm, for the different subcooling, $\Delta T_{\text{sub}} = 80$, 50, 20 and 5 °C. From this figure we find that $q_{\max}$ at low ΔT_{sub} and low u_j needs a longer time than at high ΔT_{sub} and high u_j. The reason is that the film boiling region in the leading edge appears earlier for low ΔT_{sub} and low u_j, which means that surface wetting is greatly delayed and hence the appearance

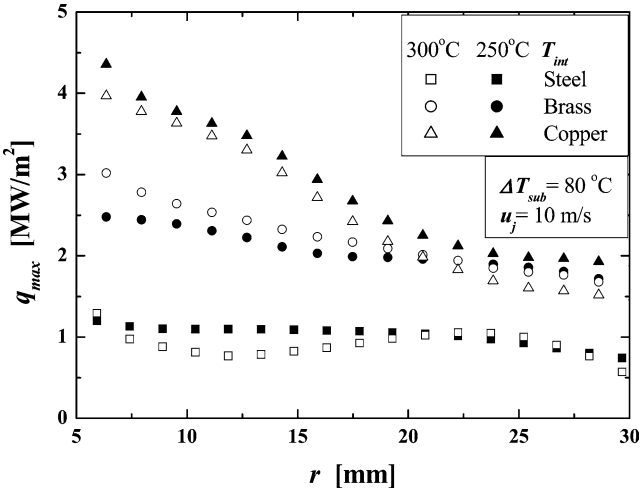

Fig. 11. Effect of material and initial temperature on the maximum surface heat flux.

of the maximum heat flux condition is also delayed. At the stagnation zone a thick vapor layer is established because the low ΔT_{sub} liquid evaporates once it strikes the high surface temperature and the low jet velocity, u_j, does not feed sufficient liquid to wet the surface. After a period of time T_w decreases to the value at which $q_{\max}$ occurs.

Fig. 13 shows the difference between the surface temperature at which the maximum heat flux occurs and the saturated temperature, $(T_w^* - T_{\text{sat}})$, as a function of $q_{\max}$ for the copper and brass at $T_{\text{int}} = 300\,^{\circ}\text{C}$, $u_j = 10\ \text{m}\cdot\text{s}^{-1}$ and two different subcooling $\Delta T_{\text{sub}} = 20$ and 50 °C. In Fig. 13 we can see that the maximum heat flux occurs when $(T_w^* - T_{\text{sat}})$ decreases to the range of 35 to 75 °C for brass, and to the

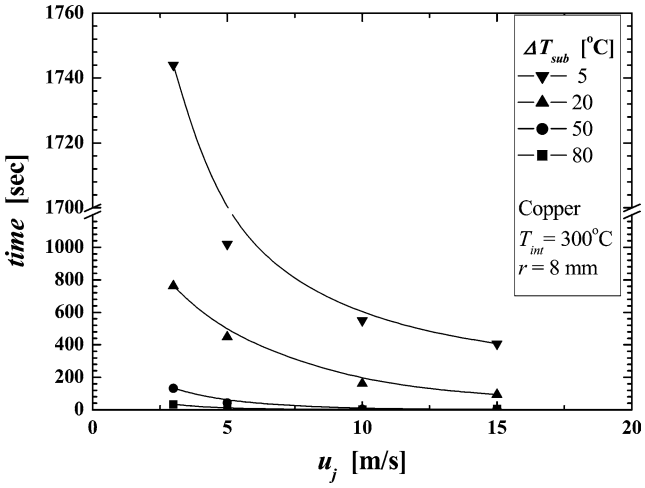

Fig. 12. Time at which maximum surface heat flux occurs.

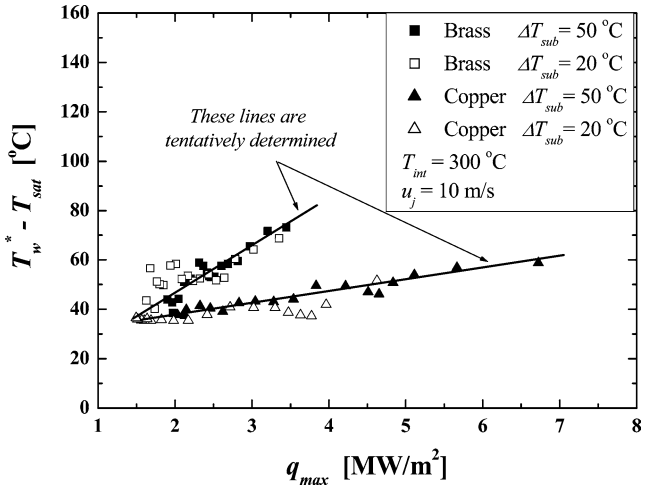

Fig. 13. The relation between maximum surface heat flux and surface temperature.

range 35 to 60 °C for copper. The difference in the slope between the two lines shows that the thermal properties of the material have an effect on T_w^* value. Fig. 13 also shows that the maximum heat flux decreases with decreasing surface temperature, T_w^*, during wetting front movement over the hot surface. The data of the other conditions shows almost the same behavior of that illustrated in Fig. 13.

Based on the current study, the characteristics of quenching phenomenon becomes more clear than before by observing the liquid behavior over the hot surface using high speed video camera and, at the same time, estimating the surface temperature and heat flux from the solid side by using two dimensional inverse solution method. In reverse to what have been found by many researchers [9–15], we could prove that the maximum heat flux occurs in the wetted area. Interestingly, we found that the maximum heat flux occurs when the surface temperate decreases to a value less than 170 °C for all carried experiments. Heat transfer coefficient, which has gained weak attention by other researchers especially in two-phase flow process, was calculated during the quenching and the location of the maximum heat transfer coefficient on the surface could be determined. There still a need to go in deep to clarify the above analyzed characteristics, and we hope to handle this issue in future work.

5. Conclusions

(1) The surface temperature and heat flux seem physically reasonable over the whole surface using the two-dimensional inverse heat conduction solution.
(2) In reverse to what have been found by many researchers, we could prove that the maximum heat flux occurs neither in the wetting front, nor in the boiling region.
(3) Maximum surface heat flux, $q_{\max}$, does not start at the same time that the jet water strikes the heated block; it is observed to start when surface temperature, T_w, decreases to a value less than 170 °C.
(4) The time that is needed to start the maximum heat flux over the heated surface is longer at a condition of low subcooling and low jet velocity than at a condition of high subcooling and high jet velocity.

References

[1] J. Filipovic, R. Viskanta, F.P. Incropera, T.A. Veslocki, Thermal behavior of a steel strip cooled by an array of planar water jets, Steel Res. 63 (1992) 438–446.
[2] C. Köheler, E. Specht, R. Jeschar, Heat transfer with film quenching of vapourizing liquids, Steel Res. 61 (1990) 553–559.
[3] C. Köheler, E. Specht, R. Jeschar, J. Slowik, G. Borchardt, Influence of oxide scales on heat transfer in secondary cooling in the continuous casting process, Steel Res. 61 (1990) 295–301.
[4] T.A. Deiters, I. Mudawar, Optimization of spray quenching for aluminum extrusion, forging, or continuous casting, J. Heat Treatment 7 (1989) 9–18.
[5] M. Ishii, Study on emergency core cooling, Br. Nuclear Energy Soc. J. 14 (1975) 237–242.
[6] J.J. Carabjo, A study on the rewetting temperature, nuclear eng. design, rusion, forging, or continuous casting, J. Heat Treatment 84 (1984) 21–52.
[7] Z.-H. Liu, J. Wang, Study on the film boiling heat transfer of water jet impinging on high temperature flat plate, Internat. J. Heat Mass Transfer 44 (2001) 2475–2481.
[8] W. Timm, K. Weinzierl, A. Leipertz, Heat transfer in subcooled jet impingement boiling at high wall temperatures, Internat. J. Heat Mass Transfer 46 (2003) 1385–1393.
[9] J. Filipovic, F.P. Incropera, R. Viskanta, Quenching phenomena associated with a water wall jet: I. Transient hydrodynamic and thermal conditions, Experimental Heat Transfer 8 (1995) 97–117.
[10] S.S. Dua, C.L. Tien, An experimental investigation of falling-film rewetting, Internat. J. Heat Mass Transfer 21 (1978) 955–965.
[11] Y. Barnea, E. Elias, Flow and heat transfer regimes during quenching of hot surfaces, Internat. J. Heat Mass Transfer 37 (1994) 1441–1453.
[12] T. Ueda, M. Inoue, Rewetting of a hot surface by a falling liquid film-effects of liquid subcooling, Internat. J. Heat Mass Transfer 27 (1984) 999–1005.
[13] V.K. Dhir, R.B. Duffey, I. Catton, Quenching studies on a zircaloy rod bundle, Trans. ASME J. Heat Transfer 103 (1981) 293–299.
[14] S. Kumagai, S. Suzki, Y. Sano, M. Kawazoe, Transition cooling of a hot metal slab by an impinging jet with boiling heat transfer, ASME/JSME Thermal Eng. Conf. 2 (1995) 347–352.

[15] Y. Mitsutake, M. Monde, Heat transfer during cooling of high temperature surface with an impinging jet, Heat and Mass Transfer 37 (2001) 321–328.
[16] M. Monde, H. Arima, W. Liu, Y. Mitutake, J. Hammad, An analytical solution for two-dimensional inverse heat conduction problems using Laplace transform, Internat. J. Heat Mass Transfer 46 (2003) 2135–2148.
[17] J. Hammad, M. Monde, H. Arima, Y. Mitutake, Determination of surface temperature and heat flux using inverse solution for two-dimensional heat conduction, Thermal Sci. Eng. 10 (2002) 17–26.
[18] X. Liu, J.H. Lienhard, J.S. Lombara, Convective heat transfer by impingement of circular liquid jets, J. Heat Transfer 113 (1991) 571–582.